

Influence of Cu-Fe alloy on the transient thermal characteristics of IMCCR under two special operating conditions

J.C. Cao^{1*}, H. Zhou¹, S. Chen², L. Shi³, J. Zhou³

¹School of Electrical engineering, Beijing Jiaotong University, Beijing, 100044 China

²School of Mechanical Engineering, Harbin University of Science and Technology, Heilongjiang, 150080 China

³Shenzhen Shineng Supernova Inc., Guangdong, 518104 China

Received June 26, 2017; Revised July 20, 2017

A novel Induction Motor with Compound Cage Rotor (IMCCR) is proposed in this paper, in which rotor bars are composed of upper parts made of Cu-Fe alloy (conductor for electric and magnetic) and lower parts made of cast aluminum. By using time-stepping Finite Element Method (FEM), the electro-thermal fields coupling analyses of IMCCR are implemented. Firstly, the electromagnetic and thermal fields of the motor under locked rotor condition are analyzed, and the transient thermal process of motor is also studied, the calculated results are validated by the experimental results. Then, the electromagnetic and thermal fields of the motor excited by impulse current are studied, and the influence on transient heat transfer process in IMCCR are analyzed, especially for the effects on stator windings insulation. The obtained results are compared with that of machine operating under locked rotor condition, which may provide references for the studies on thermal performances of machine operating with impulse current and the heat transfer characteristics of the stator winding insulation.

Keywords: Cu-Fe alloy, compound cage rotor, transient thermal field, locked rotor, inrush current.

INTRODUCTION

The novel alloy materials are widely applied to the motor. By replacing the rotor bars and the end rings of the motor, the electromagnetic parameters and the mechanical parameters are improved, thus the motor can get better performances and safer than it before. A novel alloy material, composed of copper, iron and the other elements, is developed to fabricate the rotor bars of the motor. It is conductor both for current and the magnetic field. Taking advantages of the novel Cu-Fe alloy, a novel induction motor with compound cage rotor, which is very different with the conventional motor, is developed in the paper [1,2].

In practical applications, especially in the occasion of starting with heavy load and the large voltage drop of the long wire, the motor would operate at very low speed or even under locked condition; the auto-reclosure would work. Due to the existence of residual voltage, while power is supplied again, the winding terminal voltage would exceed the rated value and the instantaneous current may ten times more than the rated ones. During the instantaneous process, the current turbulence would occur, and the harm is complicated, for example the local temperature of the motor rise sharply in such a very short time that may cause the damage of motor insulation, or even the burnt-out of the motor itself [3,4,5,6,7,8,9,10].

Thus, the novel induction motor with compound cage rotor, having high performance during starting process, is researched in the paper. The electromagnetic characteristics of the motor under locked rotor condition and operated with impulse current (2.5 times of the locked current) are analyzed. The transient thermal process of the motor under the two special conditions during 10s is also calculated. The transient temperature varies process of the stator winding insulation is detailed in the paper, which would provide reference for fault analysis about insulation in motor.

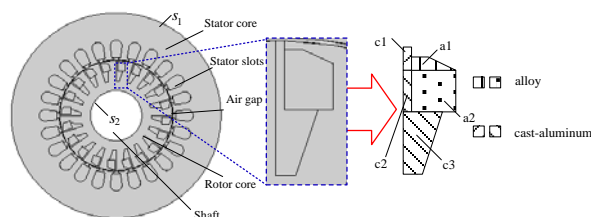


Fig.1. Structure of IMCCR and the heat equivalent diagram of the cage bar

DESIGN OF IMCCR

In this paper, the main element of the Cu-Fe alloy material is industrial pure iron (81.7% in weight) and electrolytic copper (17% in weight). Before smelting, magnesium (0.25% in weight) is put in the bottom of the mould and during the smelting process, ferromanganese (0.7% in weight),

* To whom all correspondence should be sent:
E-mail: scjcs@sina.com

copper phosphorus (0.05% in weight), ferrosilicon (0.2% in weight) and aluminum (0.3% in weight) are added in the raw materials. From associate tests, the permeability of the alloy is about 20 times than that of air and its electric conductivity is about 1.5 times than that of iron. By using the alloy material, a novel induction motor with compound cage rotor is developed. The upper part of rotor bar is made of alloy material and the lower part is made of cast aluminum. The structure of the novel IMCCR and the heat equivalent diagram of the cage bar are shown in Figure1.

ELECTRO-THERMAL ANALYSIS

Electromagnetic Analysis

To simplify the calculation of the electromagnetic field, the following assumptions the made [11]:

1)For there is no skew slot in motor and air-gap length is so small compared with motor polar pitch, the flux distribution in motor core would be 2-D perpendicular to axial direction.

2)Kelvin effect in stator core and windings is ignored.

3)Flux density, magnetic intensity, and magnetic vector potential are sinusoidal waves with time.

Based on the aforementioned assumptions, the whole cross-sectional region of motor core perpendicular to the axial direction (z-axial) is selected as the 2-D analysis model, as shown in Figure 1. The boundary of stator outer periphery s_1 and rotor inner periphery s_2 $\dot{A}_z = 0$. Thus the electromagnetic equations would be

$$\left. \begin{aligned} \frac{\partial}{\partial x} \left(\frac{1}{\mu_e} \frac{\partial \dot{A}_z}{\partial x} \right) + \frac{\partial}{\partial y} \left(\frac{1}{\mu_e} \frac{\partial \dot{A}_z}{\partial y} \right) &= js\omega\sigma\dot{A}_z - \dot{J}_z \\ \dot{A}_z |_{s=s_1+s_2} &= 0 \end{aligned} \right\} (1)$$

where \dot{A}_z and \dot{J}_z are magnetic vector potential and the source current density exclude the eddy current in the z-axial component (in A/m²) respectively, σ is the conductivity (in S/m), s is slip, μ_e is effective permeability.

In the electromagnetic analysis under locked rotor and inrush current operating condition, the stator currents are iterated calculated, in which (2) is selected as the convergence conditions.

$$\left. \begin{aligned} \dot{U} &= \dot{I}(R_1 + jx_{1e}) - \dot{E} \\ I_m^{(k)} &= I_m^{(k-1)} \frac{U}{U^{(k-1)}} \end{aligned} \right\} (2)$$

where \dot{U} is the terminal voltage(in V), \dot{E} is stator phase electromotive force(in V), I_m is winding current (in A), R_1 and x_{1e} are the windings

resistance and end leakage reactance, respectively(in ohm).

A 3kW prototype of IMCCR is produced and tested, and Table I shows the comparisons of the prototype starting performance with that of same power IM , from which the good starting performance of IMCCR could be clearly.

Table 1. Comparison of motor starting performance.

	IMCCR		Normal induction motors
	calculated	Test	Test
Starting current(A)	33.69	34.1	38.9
Starting torque(N·m)	23.68	23.7	21.6

Figure 2 shows the distributions of eddy current density in rotor bars while motor operating with locked rotor and inrush current. Comparing with that in locked rotor operating, the maximum value of induced rotor eddy current density increases about 86.3% in inrush current operating. However, the distributions tendencies have no obvious difference.

Transient Thermal Analysis

To consider the eddy loss (heat sources) distributions in rotor bars comprehensively, and make the thermal analysis model more accurately, the layered equivalent model for rotor bars is developed as shown in Figure1.

The IMCCR adopts totally-enclosed outer fan cooling system. To simplify the calculation, the 3D temperature field problem is converted into 2D situation and the solve model and temperature measured positions are shown in Figure3.

In the figure, l_1 is the inner surface of rotor core, l_2 is terminal box on the shell and the tooth ends of cooling fin, l_3 is other part on the shell. Test points S_1 and S_2 locate at stator wedges, and test points d_1 locates at stator windings, whereas test points R_1 and R_2 at casting aluminum bar and alloy bar, respectively.

According to [10], the mathematical model for 2D transient temperature field could be (3), in which the second equation is the condition of initial temperature, and the third one is the heat transmission boundary conditions, and the last equation is the adiabatic boundary conditions for shaft.

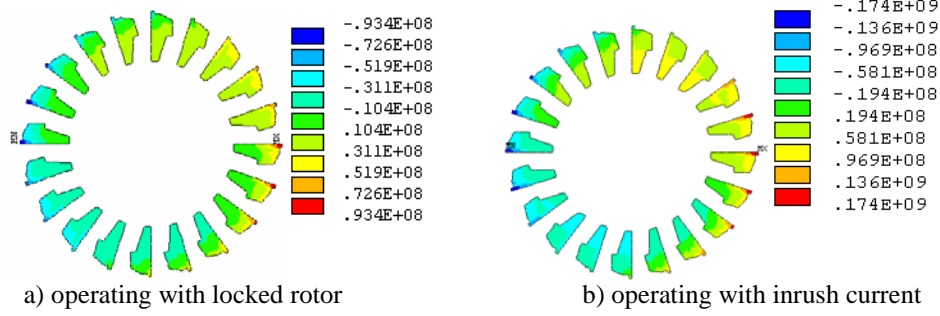


Fig.. 2. Eddy current density distribution in rotor bars (A/m²).

$$\begin{cases} \frac{\partial T}{\partial t} = \frac{1}{\rho C} \left(\lambda \frac{\partial^2 T}{\partial x^2} + \lambda \frac{\partial^2 T}{\partial y^2} \right) + \frac{q_v}{\rho C} \\ t = 0, T = \varphi(x, y) \\ -\lambda \left. \frac{\partial T}{\partial n} \right|_{l_2, l_3} = \alpha(T - T_0) \\ \left. \frac{\partial T}{\partial n} \right|_{l_1} = 0 \end{cases} \quad (3)$$

where, T is temperature (in $^{\circ}\text{C}$), λ is the thermal conductivity coefficient (in $\text{W}/(\text{m}\cdot^{\circ}\text{C})$), q_v is the heat source density(in W/m^2), ρ is the density (kg/m^3), C is mass heat capacity (in $\text{J}/(\text{kg}\cdot^{\circ}\text{C})$), t is time(in s), n is unit normal vector on the surface, α is heat transfer coefficient(in $\text{W}/\text{m}^2\cdot^{\circ}\text{C}$), T_f is the ambient air temperature (in $^{\circ}\text{C}$), $\varphi(x, y)$ is the temperature at each node when $t = 0$.

From the electromagnetic analysis, the stator copper loss and rotor eddy loss are obtained, and the corresponding heat generation rates are shown in Figure4. In the figure, d1 is for stator windings heat generation, which is determined by stator current. However, for the induced eddy current distributes unevenly in a rotor bar, the heat generation is different between parts (shown in Figure2), among which casting aluminum at rotor notch (c1) has the highest heat generation density in the motor.

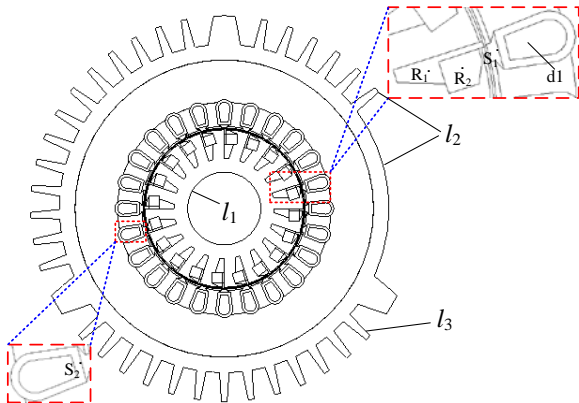


Fig. 3. Thermal analysis model and temperature test positions for IMCCR

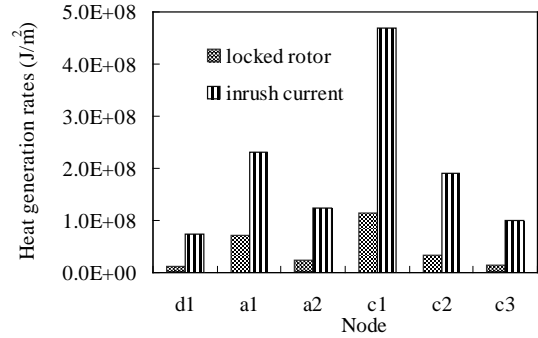


Fig. 4. Heat generation densities in IMCCR different parts under different operating

TRANSIENT TEMPERATURE ANALYSIS OF IMCCR

In this study, temperature of motor operating with short time locked rotor had been tested. The experiment equipments are shown in Figure5. Here, magnetic powder brake is selected as the simulation load. The temperature on the shell was tested by infrared thermos cope, and the temperatures inside motor are tested by heat sensitive resistance with precision of $0.1\text{ }^{\circ}\text{C}$.

Table 2. Comparison of calculated temperatures with the measured data in locked rotor operating at 10^{TH} second.

positions	calculated($^{\circ}\text{C}$)	test($^{\circ}\text{C}$)
S ₁	21.39	16.76
S ₂	21.40	17.16
R ₁	41.44	38.34
R ₂	44.72	40.52

The comparisons of test temperature with the calculated values are shown in Table. II. For equivalent model could not simulate motor actual situation completely and transient temperature measurement also have certain deviation, the calculated temperature is higher than that of measured.



Fig. 5. Experimental equipments of temperature rise

Temperature Distribution in IMCCR Stator

During the locked rotor operating and inrush current operating, the isothermals in stator slots at time of 10ths are shown in Figure 6. In locked rotor operating the highest temperature is 42.4°C, and temperature rise up about 2.9°C per second. Whereas in inrush operating, the highest temperature is about 195.5°C temperature rise rate is about 18.2°C per second, which is 6.28 times than that in locked rotor.

The temperature drop in insulation layer in locked operating is 10-25°C, whereas it is about 90-150°C in inrush operating. The highest temperature is over the extreme temperatures of insulation already, which would reduce the life of insulation.

Variation of Transient Temperature in Stator Windings

Figure7 shows the variation of temperature along the inner boundary of stator insulation layer with time. At 1st second, temperature distribution curves are nearly straight lines, and the temperature difference of insulation in locked rotor operating is only 0.8 °C, which is about 5°C in operating with inrush current. While operating for 5 second, generated heat in stator windings increase obviously, which made temperature rise significantly. The average temperature in insulation inner boundary reaches up to 89.6°C in operating with inrush current, which about 3.53 times than that in locked rotor operating. While to 10s, the average temperature reaches to 160.5°C, and the temperature difference is about 35°C, which are 36.8°C and 5.6°C for motor operating with locked rotor.

Figure8. shows the variation curves of temperature along the insulation layer outer boundary with time. Due to the poor heat transfer ability of insulation material, the heat generated in stator windings could not be delivered timely, so temperatures at these positions are comparatively lower than that in inner boundary shown in Figure7. The highest temperatures here in motors operating with locked rotor and inrush current are 15°C and 23.4°C respectively. Comparing to teeth, the heat

transfer conditions of yoke is better due to its larger area, so the temperature of insulation connect to yoke is lower than that to teeth. Thus, in Figure7 and Figure8, it is relatively lower in middle of temperature distribution curves.

From the analysis above, in the short time special operating, the temperature difference between two boundaries of insulation is so big that the temperature distribution along the radial direction is extremely uneven. Thus, radial thermal analysis for insulation layer is significantly to associate thermal stress study.

Considering the structure symmetry, only one side of insulation layer is analyzed here. From above analysis, the high temperature region of insulation includes positions at node 1, 2, 3, and 4. Thus, in following analysis, the temperature on line through node 2 and node 3 along the radial direction is studied, and temperature radial distribution in insulation layer at different time are shown in Figure9. The temperature difference in insulation layer along the radial direction is rising sharply, and the temperature changes from 1.6°C to 141.7°C in 10 second operating with inrush current, which is about 6.3 times than that of locked rotor operating, which would lead to aging or damaged for insulation.

In addition to above analysis, the thermal process of motor for the next 600 second natural cooling is also studied, as shown in Figure10. In this stage, temperature of insulation layer next to stator windings is dropping quickly, whereas for that close to stator teeth the temperature is still increasing. In the inrush current operating, temperature of insulation reaches its maximums values after 50s, and then begins to decrease, but it begins to rise after 170s due to the influence of the heat transfer from rotor. The same process of locked rotor operating is studied in [12] already.

Transient Temperature Variation in Rotor

Figure11 shows the temperature distribution of rotor in the inrush current operating. From the isotherm when $t=1s$ and $t=10s$, it can be indicated that temperature in the rotor bar increased more quickly than other parts for higher heat density here. Temperature at the notch is the highest since the higher heat flux density and bad heat transfer conditions. The temperature in rotor is decreasing gradually along the radial directing to shaft, which is similar to that in locked rotor operating studied in [12].

The highest temperatures at stator windings center (node d1) and rotor notch (node c1) are studied next, and temperature time variation curves

in locked rotor and inrush current operations are shown in Figure 12. Because the heat transfer condition at rotor notch is much better than that of stator insulation layer, temperature at rotor notch is always lower than that in windings center in locked rotor operation, although heat generation at rotor notch is

comparatively bigger. Whereas in the inrush current operation, stator windings temperature is higher than that of the rotor notch in the initial period, but temperature of rotor notch is becoming higher than that of stator windings gradually due to the high heat generation.

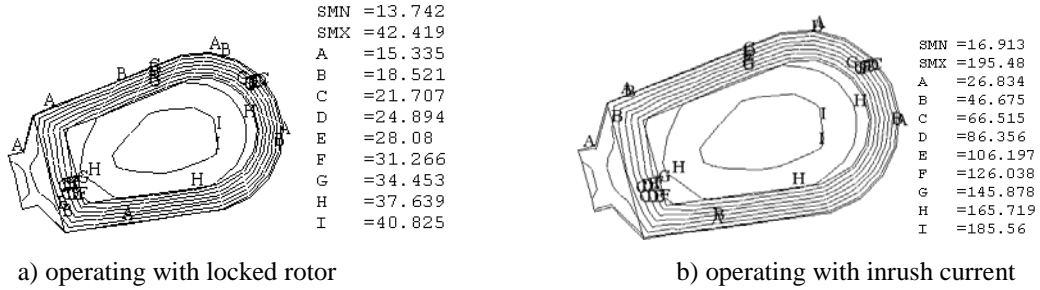


Fig. 6. Isotherm of the stator slots in IMCCR under different operating (°C).

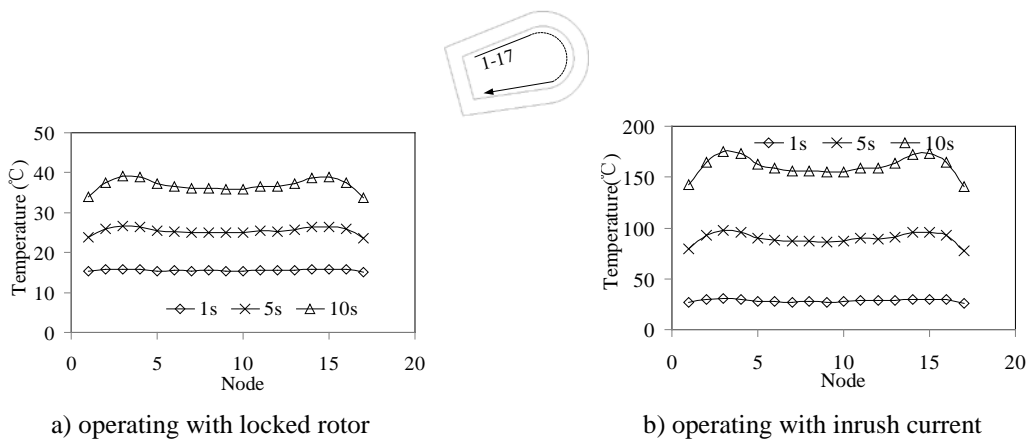


Fig. 7. Variations of temperature at insulation inner boundary with time

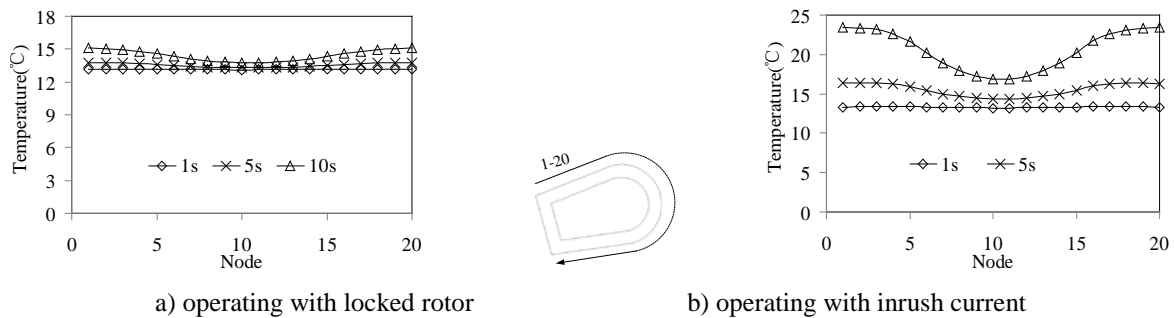


Fig. 8. Variations of temperature at insulation outer boundary with time

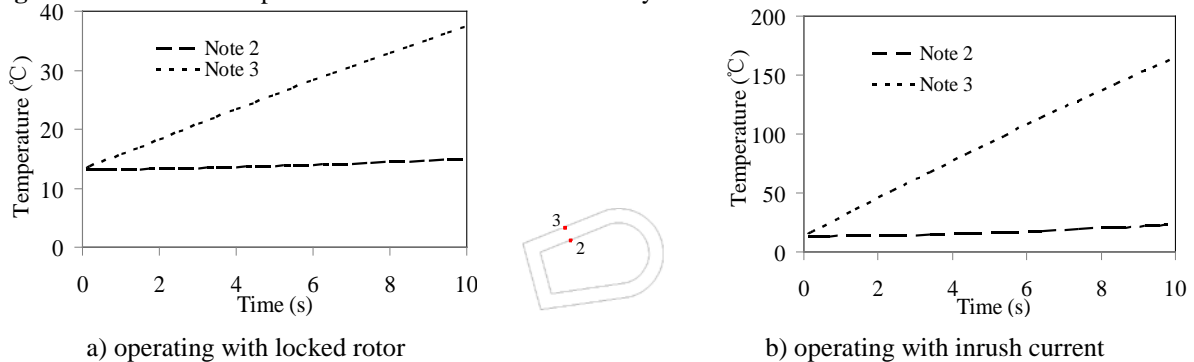


Fig. 9. Radial temperature distribution in insulation layer with time

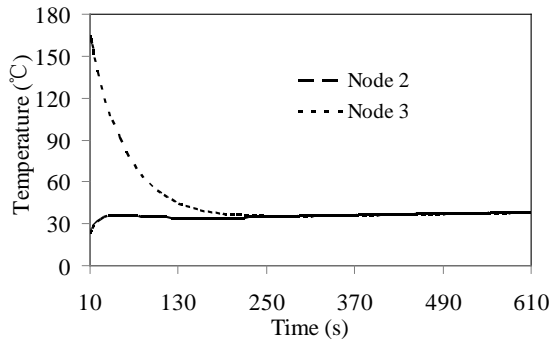


Fig. 10. Variation of radial temperature difference in insulation with time in IMCCR operating with inrush current

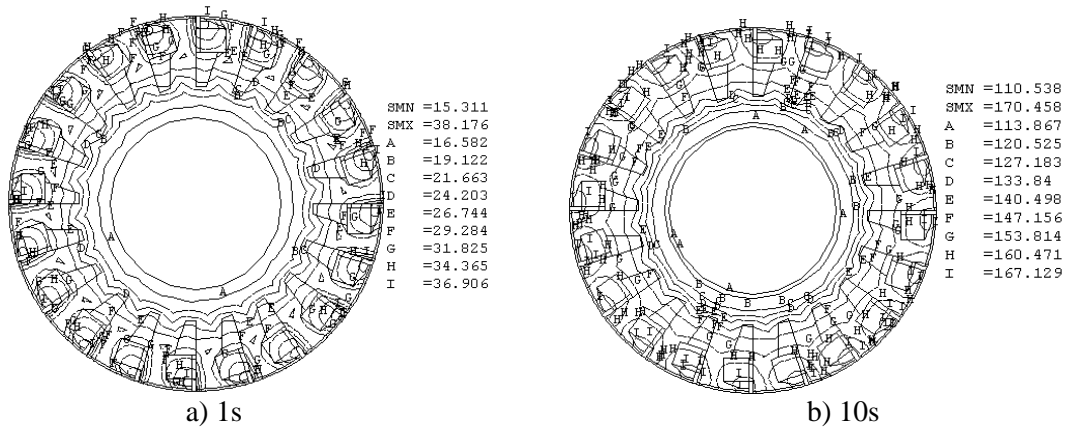


Fig. 11. Isothermal of rotor at different time in operating with inrush current

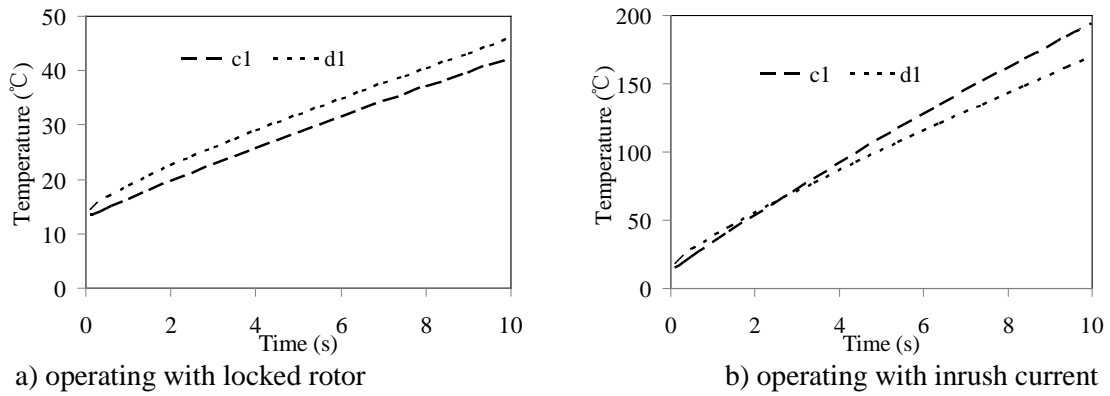


Fig.12. Variation of the highest temperature with time in IMCCR

CONCLUSIONS

1) Comparing with that in motor operating with locked rotor, the highest temperature in motor operating with inrush current appears at different position and becomes higher.

2) The temperature distributes unevenly along the inner boundary of windings insulation layer, the temperature difference is 5.6°C after locked rotor operating for 10 seconds, whereas for operating with inrush current it is about 35°C.

3) The temperature difference in insulation layer along the radial direction is rising sharply in these two operating, which changes from 1.6°C to 141.7°C in 10 second operating with inrush current, and this would lead to aging or damaged for insulation.

Acknowledgements: This work was supported in NSFC (51577007), Supported by Beijing Natural Science Foundation(3162023), Fundamental Research Funds for the Central Universities (2015RC016)

REFERENCES

1. W.L. Li, J.C. Cao, X.C. Zhang, *IEEE Trans. Ind. Electron*, **57**, 660 (2010).
2. Y.P. Zhang, *Proc. CSEE*, **21**, 89 (2001).
3. J. Faiz, M. Ghaneei, A. Keyhani, *IEEE Trans. Energy Con.*, **14**, 101 (1999).
4. W.L. Wei, C. Sina, J. Juri, *Proc. IEEE Electric Power Conf.*, **10**, 1 (2008).
5. Y.C. Chou, A.O. Nabeel, *IEEE Trans. Energy Con.*, **24**, 848 (2009).
6. S.G. Gursharan, P. Stephen, M.H. Makhlof, *IEEE Trans. Indu. Appl.*, **3**, 967 (1999).
7. R.C. Zowarka, T.J. Hotz, J.R. Uglum, H.E. Jordan, *IEEE. Trans. Magn.*, **43**, 275 (2007).
8. M.H. Zhong, H.Q. Sheng, Z.L. Min, H.J. Dong, *Electric machines & control application*, **32**, 3 (2005).
9. J. Faiz, B. Ganji, C.E. Carstensen, *IEEE. Trans. Magn.*, **45**, 2927 (2009).
10. J. Xypteras, V. Hatzianthassiou, *IEEE Trans. Energy Con.*, **14**, 996 (1999).
11. Y.Q. Tang, *Electromagnetic Field in Electric Machine*. Beijing, China: Science Press, 1998.
12. J.C. Cao, W.L. Li, F.Y. Huo, P. Cheng, J.F. Shen, *Proc. EUROCON '09*, **8**, 696 (2009).